Polish J. Chem., **76**, 419–433 (2002)

Thermal and Near-IR Photochemical Generation of Polarons in m-Nitroaniline Crystals. Application of 2D Correlation FT-NIR Spectroscopy*

by M.M. Szostak[1] and M.A. Czarnecki[2]

[1]*Institute of Physical and Theoretical Chemistry, Wrocław University of Technology Wybrzeże Wyspiańskiego 27, 50-370 Wrocław, Poland*
[2]*Faculty of Chemistry, University of Wrocław, F. Joliot-Curie 14, 50-383 Wrocław*

(Received June 13th, 2001; revised manuscript November 5th, 2001)

Polarized FT-NIR spectra of m-nitroaniline single crystals in the 4200–10500 cm^{-1} region, non-irradiated and irradiated at 9700 cm^{-1}, corresponding to the -NH_2 stretching second overtone (3 $\nu^{s}_{NH_2}$), were recorded from 300 to 380 K. Direct heating from 325 K to 365 K (phase transition) caused an elevation of the relative background absorbance (ΔA) near 10500 cm^{-1}. The irradiation by low intensity NIR and a subsequent heating resulted in a different increase of ΔA than in the case of non-irradiated sample. The background elevation is supposed to origin from low-lying electronic transitions of radical ions (polarons) generated by irradiation and heating. Our results indicate that the polarons produced photochemically and thermally are different. The 2D correlation analysis was applied to facilitate the band assignment in the NIR region and to throw more light on thermally induced instabilities in the crystal.

Key words: meta-nitroaniline crystal, polarized near infrared spectra, near IR photochemistry, two-dimensional correlation analysis

Collective electronic excitations in solid radical ions, called polarons, produce more pronounced nonlinear optical susceptibilities than those in neutral species (neutral solitons) in conjugated polymers [1,2] as well as in the m-nitroaniline (m-NA) crystals [3]. Electrical conductivity of polyanilines [4,5,6], polythiophenes [7,8,9] and *trans*-polyacetylene [9,10] results mainly from polarons – charge carriers with spin of 1/2. Polarons are responsible for electronic absorption inside the energetic gap, known as the conductivity band in near infrared (NIR) region [1,2,10]. In turn, NIR electronic absorption occurs in the dimer radical cations of benzene, toluene [11], biphenyl, p-terphenyl, *trans*-stilben and many other hydrocarbons obtained by warming of γ-irradiated, frozen glassy solutions [12]. Also in the 1–2 μm region the electronic transitions between quinone and semiquinone sites in the same molecule are observed in solution of polyacenoquinone radical anions [13]. In crystals or polymers similar transitions occur between the π systems forming stacks [14]. On the other hand, NIR absorption may be due to vibrational excitations of first and second ν_{XH} stretching overtones, like in the p-NA [15,16] and m-NA [17] single crystals, in alcohols [18,19] and in N-methylacetamide (NMA) [20]. In order to identify temperature ranges of

* Dedicated to the memory of Professor Krzysztof Pigoń.

monomers, dimers and higher oligomers appearance in NIR spectra, the 2D correlation analysis was applied [18,19,20]. The NIR region was also explored in site-selective photochemistry, *e.g*. to study the proton transfer (PT) from nitromethane to D_2O solvent stimulated by ν_{CH} overtone excitation [21] and the H/D exchange in cobalt(III)–amine complex ion solution, where in the 700–1100 nm range both d-d electronic transition and NH stretching second overtones occur [22]. The photoizomerization of matrix-isolated oxalic acid was recently studied by the excitation in the first overtone OH stretching mode [23].

Optical nonlinearity manifestations in the vibrational spectra of m-NA single crystals were examined in our Laboratory in the fundamentals [24], lattice [25], and overtones [17] regions and the relation between vibronic couplings in vibrational spectra and optical nonlinearity was found [26]. This relation was confirmed by A. Painelli in donor-acceptor dimers by the two-state model extended to include electron-phonon coupling [27]. The study of polarized resonance Raman spectra of m-NA revealed radical ions generation by the 532 nm laser line and the intermolecular charge transfer [28]. Polarized IR reflection spectra with the bands reaching up 30% of reflectance indicated "metallic" or ionic character of this material [29]. Urbański *et al.* detected weak electric conductivity and paramagnetic species in the solid m-NA by EPR spectroscopy [30]. Asaji and Weiss observed an abnormal current during pyroelectricity study above 350 K [31]. In our studies EPR signals were recorded in the m-NA crystals irradiated in the conventional spectrometer for several hours (*e.g*. 72 h) in the region of -NH_2 overtones and then annealed at 323 K [32,33]. Besides an anomalous contraction, at 330 K some discontinuities on thermal expansion curves and the background increase with other changes in the overtone spectra were observed [32]. These findings have been explained by a photochemical reaction in the NIR range, connected with the vibrationally induced PT's and subsequent formation of, at least, two kinds of unpaired spins [32,33]. Due to further investigations of molecular motions in the m-NA crystal, two phase transitions and the plasticity growing with temperature were detected. The presence in ground samples of paramagnetic species and their generation by polychromatic low energy radiation was proved by the temperature dependence of spin-lattice relaxation time (T_1), by means of ^{1}H-NMR pulse method. The same results, together with the temperature dependence of second moment, evidenced the 180° jumps of -NH_2 group protons starting at about 320 K. Above 320 K an electrical conductivity contribution appeared in the imaginary part of electrical permittivity (ε") at low field frequencies [34]. The fluorescence spectrum, unusually red shifted with respect to the phosphorescence one, stemmed from radical ions generated mechanically by rapid freezing of samples and photogenerated by UV [3].

In this paper the FT-NIR spectra of m-NA crystals at various temperatures are presented in order to separate the effects of direct heating from those of the NIR irradiation and to throw more light on the polarons formation induced by the proton jumps and by the NIR irradiation. The second purpose of the present study is the assignment of bands in the NIR region. In order to facilitate this operation we applied 2D correlation analysis [18,19,35].

EXPERIMENTAL

Single crystals of m-NA were obtained from the zone refined material by the Bridgman method and their crystal structure [36] was verified by X-ray diffraction. Five samples in the form of ~ 5 × 5 mm^2 plates of different thickness (0.1 ÷ 0.8 mm) parallel to (010) plane were used. The samples were oriented under a polarizing microscope and then the polarized spectra were measured on a Perkin-Elmer FT 2000 spectrometer. A Perkin-Elmer heatable vertical liquid cell was adapted to measure crystal spectra at various temperatures with accuracy of ±2 K. The spectra were recorded with 4 cm^{-1} resolution and 32 scans were accumulated. The polarized spectra were measured in the 4200–10500 cm^{-1} range. The variable temperature spectra were measured at polarization **E** ⊥ **a** for sample 2 and for the next three samples at **E** ⊥ **c**. Polarized spectra for sample 4 were measured at room temperature, then the sample was irradiated for one hour at 1.03 μm (~9700 cm^{-1}) in the NIR spectrophotometric unit with tungsten lamp. The slit width of SPM-2 monochromator was set to 0.5 mm. After irradiation the polarized spectra at room temperature were recorded again. Next, the measurements at polarization **E** ⊥ **c** were performed at different temperatures. The direction **E** ⊥ **c** was chosen for the majority of records since it is the polar axis of the crystal [36].

The variations in background absorption upon temperature elevation were measured as relative absorbances (ΔA) *i.e*. the difference between the absorbance (A) at 10500 cm^{-1} and at 6250 cm^{-1} (the smallest A in the spectra). 2D correlation analysis was performed using MATLAB software (The Math Works Inc.) and the computational algorithm was based on the Hilbert transformation of the dynamic spectra [35].

RESULTS AND DISCUSSION

Assignments: In Fig. 1 the polarized spectra in the region of combinations (4200–5200 cm^{-1}), in the first overtones of CH and $–NH_2$ stretching vibrations (5500–7000 cm^{-1}) region and in the second overtones (8500–10500 cm^{-1}) range are shown. The analysis of the 2D correlation spectra shown in Fig. 2 enabled to assign more bands in the 5500–7200 cm^{-1} range than it was proposed previously [17]. Two peaks at 6612 and 6692 cm^{-1} are correlated with the peaks at 5940, 5964 cm^{-1} and with the wide spectral feature between 6060 and 6078 cm^{-1} (Fig. 2A). The wavenumbers 6612 and 6692 seem to correspond to combinations $\nu^{as}_{NH_2} + \delta^{s}_{NH_2}$ and $\nu^{as}_{NH_2} + \nu^{s}_{NH_2}$, respectively. These two combination vibrations belong to symmetry species B_1 in the C_{2v} local ($-NH_2$) point group and are polarized along the **c** axis [29]. This is probably the reason that their intensities grow synchronously with temperature increase below the phase transition in the **c** polarized spectrum, in contrast to the bands of $2\nu^{as}_{NH_2}$ at 6794 cm^{-1} and at 6583 cm^{-1} belonging to A_1(**a**), that are absent in Fig. 2A. The bands near 6000 cm^{-1} correspond to the ten overtones and combinations of the four ν_{CH} fundamentals of A' symmetry [29]. The spectrum in Fig. 2B reveals asynchronicity with T increase between bands at 6692, 6612 cm^{-1} and the 6078 cm^{-1} band.

In the region 4200–5500 cm^{-1} (Fig. 1A) only three bands have been previously assigned [17]. Fig. 3 shows the synchronous and asynchronous correlation between 5500–7200 cm^{-1} and 4200–4800 cm^{-1} regions and in Fig. 4 the correlation in the region 4200–4800 cm^{-1} is shown. The strong band at ~5030 cm^{-1} is excluded from the correlations as it obscures the weaker bands. As it is seen, the bands between 4200–4400 cm^{-1} are correlated to the ν_{CH} combinations at ~6000 cm^{-1} as well to bands in the 6500–7000 cm^{-1} region (Fig. 3A). Simultaneously, no asynchronous peaks in this region (Fig. 3B) appear. It suggests that in the 4200–4400 cm^{-1} range the

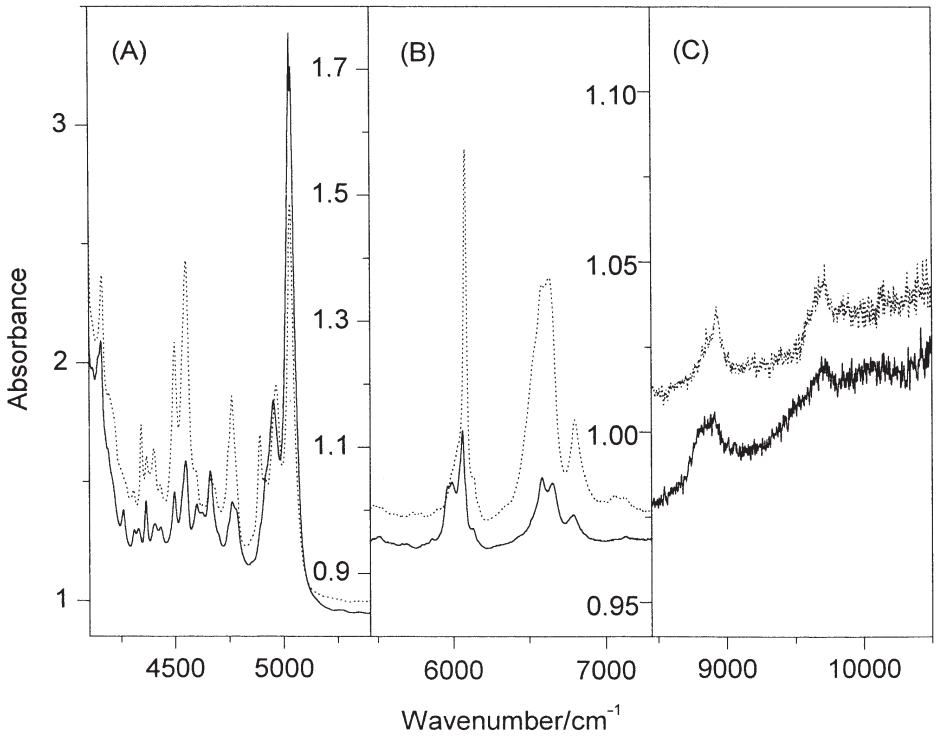

Figure 1. Polarized NIR spectra of the m-NA single crystal at room temperature: A) in the region of combinations, B) first overtones of CH and NH_2 vibrations, C) second overtones of CH and NH_2 vibrations; dashed line: **E a**, solid line: **E c**.

combinations of the $-NH_2$ group with those of the phenyl ring vibrations occur. The intensity change at 4570 cm^{-1} is strongly correlated with the intensity changes of all bands in the 5500–7200 cm^{-1} region and with the background increase (Fig. 3A). The proposed assignments are assembled in Table 1.

The effect of temperature and NIR irradiation on the polarized NIR spectra: NIR irradiation and heating, each of the stimulus separately, as well as the heating just after the irradiation affect the polarized NIR spectra of the m-NA crystal in different ways.

1. The irradiation at 1030 nm for 1 hour in the dispersive spectrometer increases the spectrum background in the whole region (Fig. 5). The change is greater in the spectra polarized parallel to the **a** axis (**E a),** $\Delta A = 0.50$ absorbance unit, than in the polarization **E c,** $\Delta A = 0.33$ absorbance unit.

2. Direct heating causes the background elevation above 7000 cm^{-1} (Fig. 6). The maximum increase of the background, measured at 10500 cm^{-1}, is significantly higher at the polarization **E c** – 60 % (Fig. 6A) than that at the polarization **E a** – 8% (Fig. 6B). The ΔA is growing from 325 K to the phase transition temperature (365 K) and then it rapidly decreases (Fig. 7). The band positions between 5500–7200 cm^{-1} shift slightly with increase in T identically for the irradiated and nonirradiated samples.

The positions of the $2\nu^{s}_{NH_2}$ and $2\nu^{as}_{NH_2}$ bands increase at the rates 0.07 $cm^{-1}K^{-1}$ and 0.14 $cm^{-1}K^{-1}$, respectively, while the positions of $\nu^{as}_{NH_2} + 2\delta^{s}_{NH_2}$ and ν_{CH} combinations bands decrease.

3. Heating of the irradiated sample 4 changes ΔA to lesser extent than in the case of the nonirradiated sample. In addition, at 365 K no discontinuity is observed. Instead, at about 380 K ΔA falls to the same level like as that at room temperature (Fig. 7).

The 2D synchronous correlation (not shown) indicates an increase in the band intensities in the region of the first overtones in phase with the background increase and from the corresponding asynchronous correlation it results that the rate of the intensity changes near 6060 cm^{-1} is different from the rate of background increase. The comparison of the diagonal spectra of synchronous correlations (so called power spectra) for samples 5 and 4 reveals small differences in intensity and significant in position changes with T, before and after irradiation, below the phase transition (Fig. 8). Detailed examination yields the different values of some band positions for

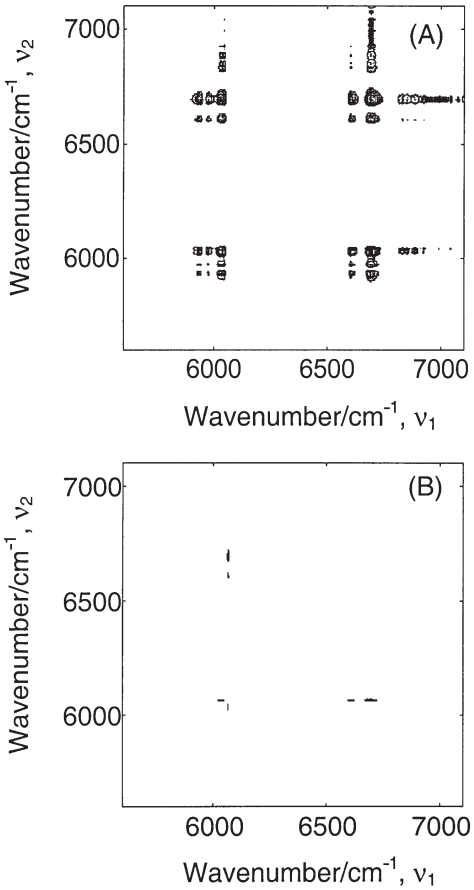

Figure 2. 2D correlation spectra in the region of first overtones in the temperature range below the phase transition (300–365 K), (A) – synchronous correlation, (B) – asynchronous correlation. Spectrum at 300 K was taken as the reference.

nonirradiated/irradiated samples: 6044/6028 and 6612/6604 cm^{-1}. The distinct minimum corresponding to the $2\nu_{CH}$ band lies at 6060 cm^{-1} for nonirradiated sample and at 6068 cm^{-1} for irradiated one. Above the phase transition temperature (Fig. 9) the bands connected with $–NH_2$ overtones disappear from the spectra of both nonirradiated and irradiated samples, while the –CH bands change their shapes and intensities. The background at 10500 cm^{-1} increases strongly in the nonirradiated sample (Fig. 9A) in contrast to the irradiated sample (*cf.* the abscissa scales).

The increase in the spectral background shown in Fig. 5, caused by the irradiation at 9700 cm^{-1} ($3\nu^{s}_{NH_2}$; 116,0 kJ/mol), is probably induced by the intermolecular proton transfer from the $–NH_2$ group to the $–NO_2$ group along the weak hydrogen bonding (HB). The small number of paramagnetic species, presumably polarons, estimated in the ground state at room temperature as equal 10^{15} g^{-1} in [30] and 10^{15} cm^{-3} in [34] could absorb the same radiation and due to the electron-phonon coupling could produce new polarons. It may be a case of autocatalysis, because of induction times re-

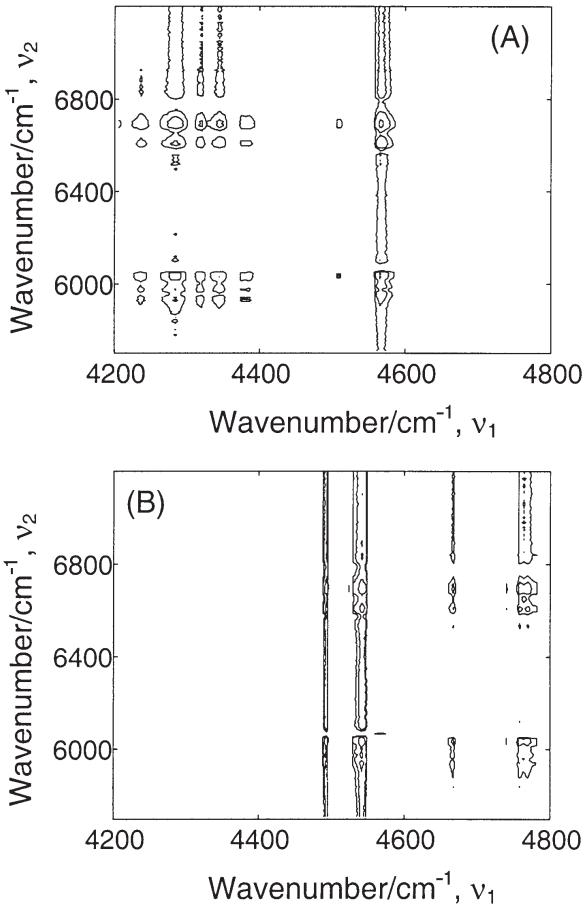

Figure 3. 2D crosscorrelation spectra between the regions of first overtones and combinations below the phase transitions, (A) – synchronous correlation, (B) – asynchronous correlation.

vealed by the recent measurements of m-NA Raman spectra as function of NIR exposure time [37]. The elevation of the background is stronger in the **a** polarization than in the **c** one. On one hand, this agrees with the direction of $3\nu^{s}_{NH_2}$ transition dipole moment [24] and on the other hand it indicates that the presumed electronic transition is also **a** polarized. If it is so, the electronic absorption may be connected with a n-π* transition, polarized in the phenyl ring plane [24] and connected with the $–NH_2$ or/and $–NO_2$ chromophores, leading to a charge separation.

Self complexes of zwitterions in the m-NA crystal at room temperature were already proposed, when rationalizing its EPR spectra [30]. The zwitterion constituted one limiting structure of m-NA in the first hyperpolarizability (β) calculation, when searching for molecular reason of optical nonlinearity [38]. It is supposed that both proton transfer and collective electronic transitions could induce zwitterions formation. The presence of charged species in the ground state and their easy generation by NIR irradiation is consistent with the ionic character of the m-NA crystal, revealed by the reflection spectra [29].

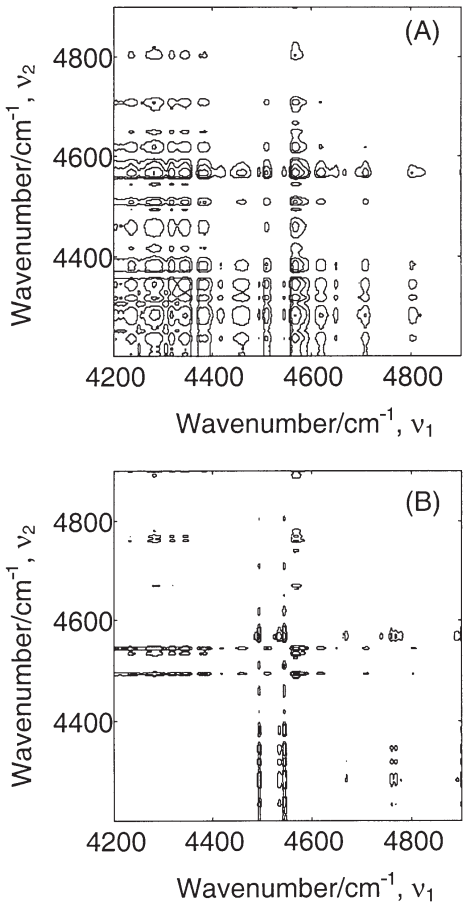

Figure 4. 2D correlation spectra in the region of combinations without the strongest band (5030 cm^{-1}), (A) – synchronous correlation, (B) – asynchronous correlation.

Table 1. Assignments of overtone and combination bands in the m-nitroaniline crystal.

Wavenumbers					
in unpolarized spectra	in 2D correlation spectra	in polarized spectra		Observed dichroism	Proposed assignments
		E||a	**E||c**	$R_{c/a}$	
			4259	>>1	$\nu^{s}_{NH_2} + \gamma_{CH}$ (ν_{17b})
4308		4306	4309	~1	$\nu^{s}_{NH_2} + \delta^{as}_{NH_2}$
			4329	>>1	
4341		4341		<<1	$\nu^{s}_{NH_2} + \delta_{CH}$ (ν_{18b})
4364		4366	4364	>1	$\nu^{s}_{NH_2} + \gamma_{CH}$ (ν_{17b})
4401		4400	4406	<1	$\nu^{s}_{NH_2} + \delta_{CH}$ (ν_{9b})
		4428	4431		
4497		4497	4496	<<1	$\nu^{s}_{NH_2} + \delta_{CH}$ (ν_{3})
	4570				
4551		4551	4549.5	<<1	$\nu^{s}_{NH_2} + \nu_{CN\,(H_2)}$
4597		sh	4600	>1	
4663		4667	4663	≥1	$\nu^{as}_{NH_2} + \nu_{CN\,(H_2)}$
4762		4761	4763	<<1	$3\delta^{s}_{NH_2}$
4892		4890	sh	<<1	$\nu^{s}_{NH_2} + \delta^{s}_{NH_2}$
4958		4966	4952	~1	$\nu^{s}_{NH_2} + \nu_{8a}/\nu_{8b}$
			5027		$\nu^{as}_{NH_2} + \nu_{8a}/\nu_{8b}$
5030		5030		>1	
			5034		$\nu^{as}_{NH_2} + \delta^{s}_{NH_2}$
	5940			>1	
			5957		
	5964			>1	I overtones and
5973		5987	5988		combinations
6061	6060		6059	>1	of ν_{CH}
	6078	6078		<1	
6123		6132	6128	<1	
			6509	<<1	$\nu^{s}_{NH_2} + 2\delta^{s}_{NH_2}$
6583		6586	6583	<<1	$2\nu^{s}_{NH_2}$
	6612				
6652		6634	6653	<1	$\nu^{as}_{NH_2} + 2\delta^{s}_{NH_2}$
	6692				$\nu^{s}_{NH_2} + \nu^{as}_{NH_2}$
6793		6798	6789	<1	$2\nu^{as}_{NH_2}$
8914		8927	8913		II overtones and combinations of ν_{CH}
9707		9717	9694	<1	$3\nu^{s}_{NH_2}$

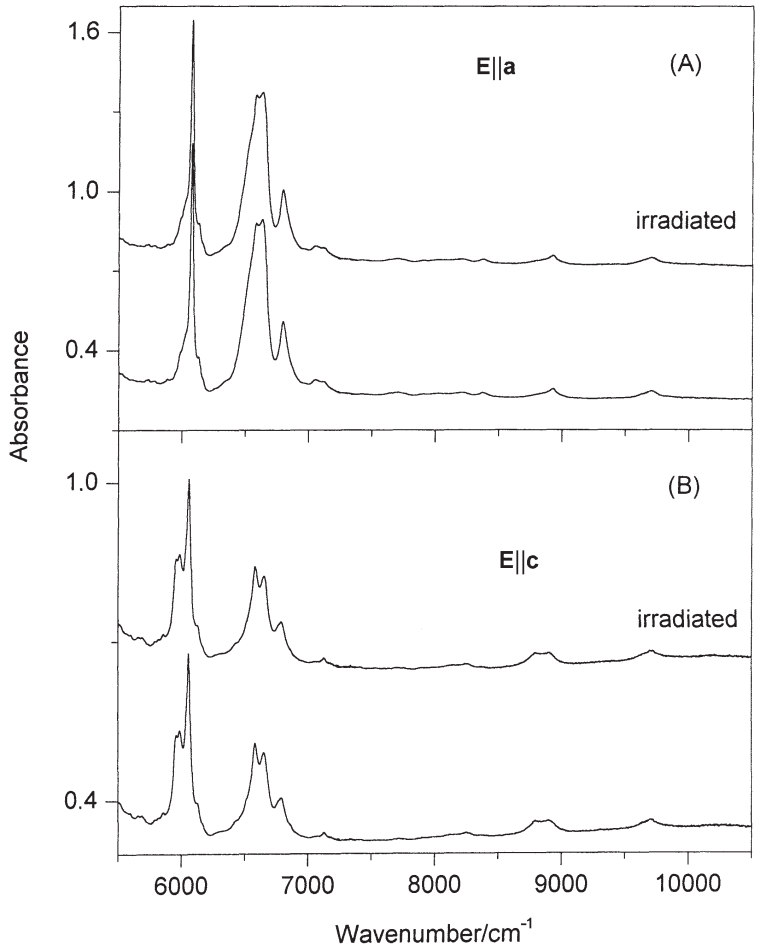

Figure 5. Polarized spectra of the m-NA (sample 4) before (lower curve) and after (upper curve) irradiation at λ = 1030 nm in dispersive spectrophotometer for 1 hour; A) **E a**, B) **E c**.

Ionic species could enhance the strength of HB [39]. Hydrogen bonding in the m-NA crystal is very long, $d_{NH..O}$ = 3.24 Å [36], longer than in the p-NA crystal ($d_{NH..O}$ = 3.07 Å) [40].In contrast to that, the red shifts of the $-NH_2$ stretching vibrations band in crystal with respect to solution spectra are smaller in p-NA [41] than in m-NA [24], indicating the stronger HB in the latter. The observed discrepancy from the relationship between NH stretching wavenumbers and N...O distances in the m-NA crystal is similar to that in the NMA one [42]. It seems to confirm the ionic species existence connected with proton transfer, as it was found in the NMA crystal at low temperature [43]. The deformation band $\delta^{s}_{NH_2}$ is in the m-NA spectra unexpectedly red shifted, when going from solution to crystal. It may results from the bifurcation of HB in the m-NA crystal [44] or/and from the ionic surroundings. Ionic species could also augment the asymmetry of HB [39,43]. The asymmetry of HB in the m-NA crystal mani-

fests itself by the monotonically decreasing second moment M_2 of the NMR line below 320 K [34], according to the theory [45]. Proton transfers in this asymmetric potential well might be able to generate semiquinone radical ions, which in meta-benzene derivatives are more reactive than in ortho- and para-semiquinones [46]. It is also supposed that the proton is transferred along the direction close to the **a** axis.

The increase of the background upon the direct heating above 320 K, much stronger in the **c** than in the **a** direction, suggests as its reason the intermolecular charge transfer along the **c** axis, observed in the polarized Raman lattice spectra [28] and/or the long range induced-dipole interactions strengthened by the permanent dipole moment of the unit cell in the **c** direction [29]. Above 320 K the 180° proton jumps give rise to the breaking of hydrogen bondings, formation of charged aggregates and electrical conductivity [34]. The reorientational disorder and dielectric permittivity, increasing with temperature [34], are beneficial for the photogeneration of charge carriers [5,8,47]. The shape and polarization of the background increase caused by heating, different from this one caused by the NIR irradiation, must be connected with different kind of polarons. It seems that they are propagating along the phenyl ring stacks parallel to the **c** axis, similarly to the electronic transitions found in the aromatic dimer cations [11,12] and in the monoclinic quinhydrone crystal [48]. The formation of the phenyl ring stacks along the **c** axis in the m-NA-room temperature phase

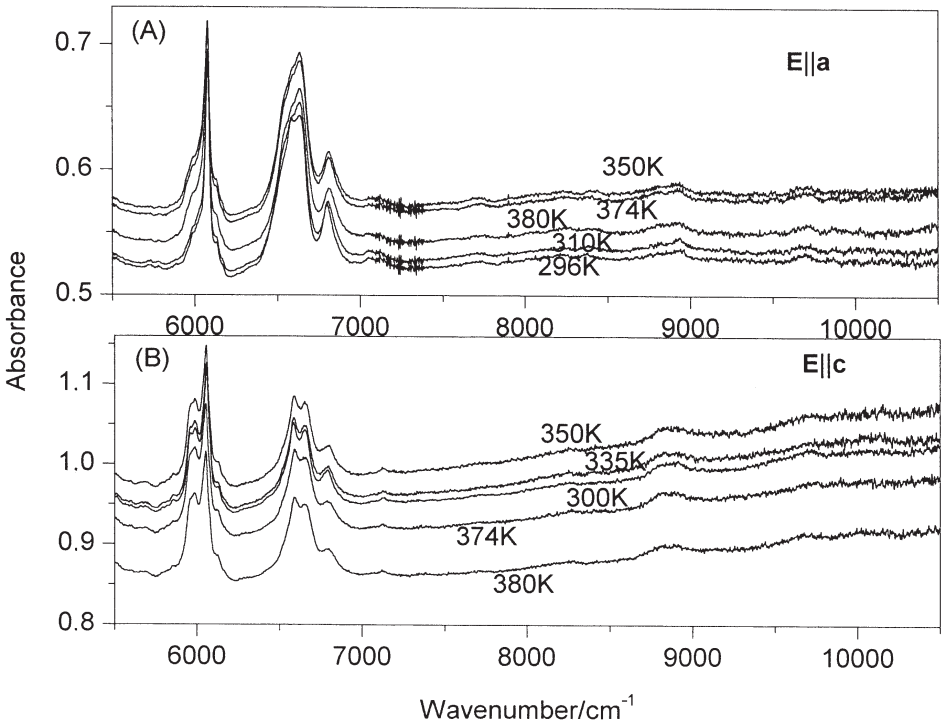

Figure 6. Polarized NIR spectra of the m-NA single crystal in the region of first and second overtones at different temperatures. A) sample 2 (**E a)**; B) sample 3 (**E c**).

is evidenced in the X-ray structure [35,49]. At 365 K the crystal becomes plastic [34], the smaller aggregates could easier recombine and the background decreases (Fig. 7). But also the sublimation of the sample at elevated temperatures cannot be excluded as the reason of the ΔA decrease. The proton or hydrogen atoms in the disordered structure could be the charge carriers like in the disordered ice, where also anomalous thermal expansion is observed [50], or like in the NMA crystal [43].

In the irradiated sample there are, as suggested, semiquinone radical ions. Their population must be significant, as it results from the ΔA smaller than in the only heated sample (Fig. 7). The smaller ΔA is the consequence of PT and probably formation of the =NH system, what excludes the $-NH_2$ proton jumps in the photogenerated species. Their presence smears the instability at 365 K, as the proton transfer may be also considered as a transformation of the solid state or a chemical reaction. The radical ions present in all m-NA solid samples at room temperature seem to play a role of an autocatalyst of the photoinduced proton transfer and it may rationalize the great difference between the heating effect of samples irradiated and nonirradiated. The temperature and pressure induced instabilities in the quinhydrone crystal have been

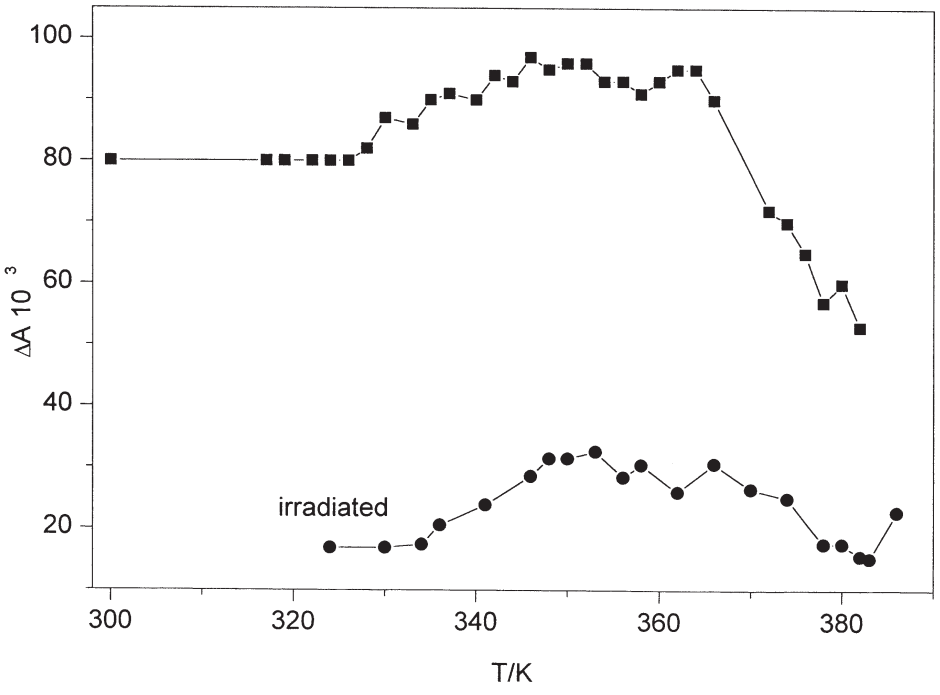

Figure 7. Temperature dependences of ΔA, the differences between the absorbances at 10500 cm^{-1} and 6250 cm^{-1} (the lowest A value): a) for the sample 5 (upper curve), b) for the sample 4 previously irradiated (lower curve). The lines are only guides for eyes.

explained by the proton transfer linked with charge transfer transition – both in different directions [48].

The appearance of the 4570 cm^{-1} band in the 2D correlation spectra (Table 1) may be attributed to the growing ionicity (with T increase), which strengthenes hydrogen bondings in the m-NA crystal. As a consequence, the positions of $-NH_2$ bands could change dramatically, like in the NMA crystal [43]. This fact might also explain the ~5030 cm^{-1} band splitting (Table 1) and the band position changes after NIR irradiation, listed previously. These features cannot be attributed now to positive or negative polarons formation. At present, the calculations of wavenumbers and intensities of vibrational bands of open shell species originating from the m-NA molecule are in progress [37], and we hope to proceed the interpretation of these observations.

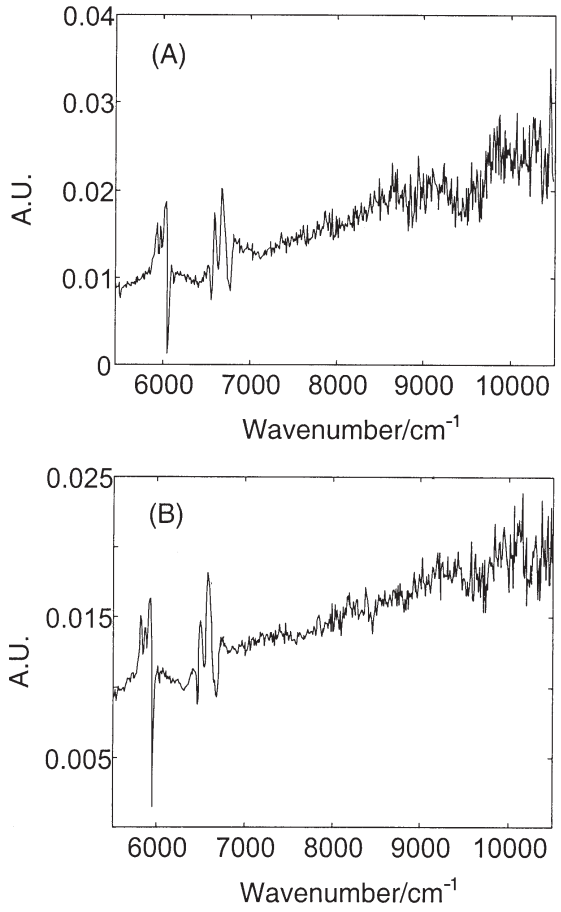

Figure 8. Power spectra in the region of first overtones in the temperature range below the phase transition (365 K), (A) – sample 5 only heated, (B) – sample 4 irradiated and subsequently heated.

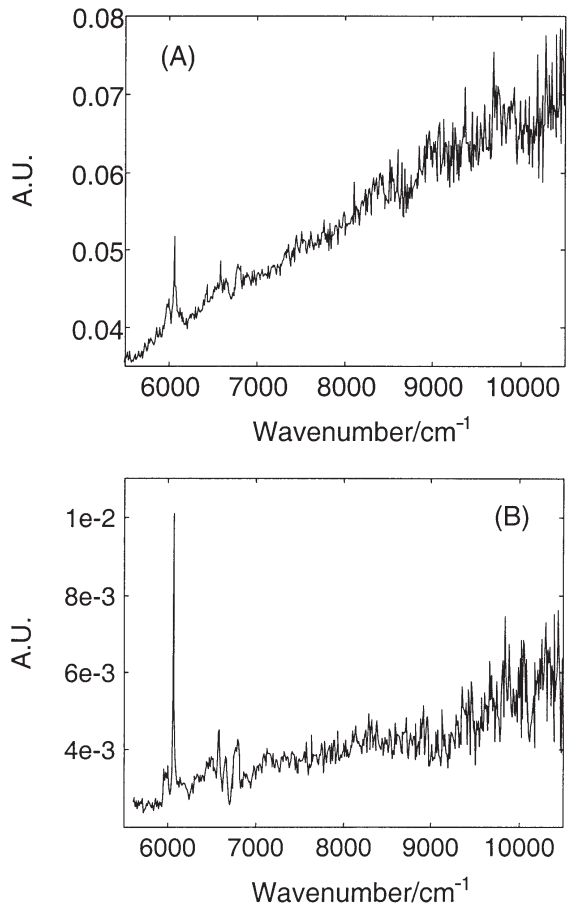

Figure 9. Power spectra in the region of first overtones in the temperature range above the phase transition (365 K), (A) – sample 5 only heated, (B) – sample 4 irradiated and subsequently heated.

CONCLUSIONS

The comparison of magnitude and direction (polarization) of background increase (ΔA) caused by: i) the NIR irradiation, ii) heating, iii) both irradiation and heating, together with previous EPR data [32,33] suggests that at least two kinds of collective excitations of unpaired spin species (polarons) are generated in the m-NA crystal. It is supposed that the intermolecular proton transfer, induced by the NIR irradiation along the asymmetric hydrogen bonding, couples with the low lying electronic transition in paramagnetic species present in all samples, what leads to the increase of the polarons population (autocatalysis) and growing absorption at about 1 μm. The polarons (and protons) propagate along the direction close to the **a** axis and are semiquinoic in nature. The temperature increase in the 320–365 K range results in

the proton jumps, hydrogen bonding breaking and the intermolecular charge transfer along the phenyl ring stacks parallel to the **c** screw axis. In the irradiated sample the formation of the =NH system excludes the $-NH_2$ proton jumps and it diminishes the heating effect of samples irradiated *vs* nonirradiated.

Acknowledgments

M.M.S. would like to acknowledge the role of Professor K. Pigoń, who first introduced the studies on nitroanilines into this laboratory. Single crystals of m-NA have been provided by his coworker, Dr. A. Cehak.

This work is sponsored by the Polish State Committee for Scientific Research, grant no 3T09A 14018.

REFERENCES

1. Takahashi A. and Mukamel S., *J. Chem. Phys*., **103**, 7144 (1995).
2. Meerholz K., Świątkiewicz J. and Prasad P.N., *J. Phys. Chem*., **99**, 7715 (1995).
3. Szostak M.M., Kozankiewicz B., Wójcik G. and Lipiński J., *J. Chem. Soc*., *Farad. Trans*., **94**, 3241 (1998).
4. Bartonek M. and Kuzmany H., *Synth. Met*., **41**–**43**, 607 (1991).
5. Cromach K.R., Epstein A.J., Masters J., Sun Y. and MacDiarmid A.G., *Synth. Met*., **41**–**43**, 641 (1991).
6. Engert C., Umapathy S., Kiefer W. and Hamaguchi H., *Chem. Phys. Lett*., **218**, 87 (1994).
7. Lanzani G., Rossi A., Piaggi A., Pal A.J. and Taliani C., *Chem. Phys. Lett*., **226**, 547 (1994).
8. Lane P.A., Liess M., Wei X., Partee J., Shinar J., Frank A.J. and Vardeny Z.V., *Chem. Phys*., **227**, 57 (1998).
9. Furukawa Y., *J. Phys. Chem*., **100**, 15644 (1996).
10. Walser A.D., Dorsinville R., Tubino. R. and Alfano R.R., *Phys. Rev*., **B 43**, 7194 (1991-II).
11. Bedger B. and Brocklehurst B., *Trans. Farad. Soc*., **65**, 2582 (1969).
12. Kira A. and Inamura M., *J. Phys. Chem*., **83**, 2267 (1979).
13. Józefiak T.H. and Miller L.L., *J. Am. Chem. Soc*., **109**, 6560 (1987).
14. Miller L.L. and Mann K.R., *Acc. Chem. Res*., **29**, 417 (1996).
15. Szostak M.M. and Rohleder J.W., *Acta Phys. Polon*., **40**, 517 (1971).
16. Szostak M.M., *Acta Phys. Polon*., **42**, 279 (1972).
17. Szostak M.M., *Mat. Sci*., VII, 359 (1981).
18. Czarnecki M.A., Maeda H., Ozaki Y., Suzuki M. and Iwahashi M., *Appl. Spectrosc*., **52**, 994 (1998).
19. Czarnecki M.A., Maeda H., Ozaki Y., Suzuki M. and Iwahashi M., *J. Phys. Chem. A*, **102**, 9117 (1998).
20. Liu Y., Ozaki Y. and Noda I., *J. Phys. Chem*., **100**, 7326 (1996).
21. Goodall D.M. and Chetwood I., *Chem. Phys. Lett*., **129**, 291 (1986).
22. Goodall M., Hollis D.B. and White M.S., *J. Phys. Chem*., **91**, 4255 (1987).
23. Façusto R. and Maçôas E.M.S., *J. Mol. Struct*., **563**–**564**, 27 (2001).
24. Szostak M.M., *J. Raman Spectr*., **8**, 43 (1979).
25. Szostak M.M., *J. Raman Spectr*., **12**, 228 (1982).
26. Szostak M.M., *Chem. Phys*., **121**, 449 (1988).
27. Painelli A., *Chem. Phys. Lett*., **285**, 352 (1998).
28. Szostak M.M., Smith B.J.E. and Batchelder D.N., Proc. XI Int. Conf. Raman Spectrosc. Eds. Clark R.J.H. and Long D.A., John Wiley & Sons, London 1988, 583.
29. Szostak M.M., Le Calvé N., Romain F. and Pasquier B., *Chem. Phys*., **187**, 373 (1994).
30. Urbański T., Kryszewski M., Kosiński K. and Sas W., *Roczn. Chemii*, **47**, 757 (1973).
31. Asaji T. and Weiss A., *Z. Naturforsch*., **40a**, 567 (1985).
32. Szostak M.M., Jakubowski B. and Komorowska M., *Mol. Cryst. Liq. Cryst*., **229**, 7 (1993).
33. Szostak M.M., Komorowska M. and Wójcik G. (unpublished results.)
34. Szostak M.M., Wójcik G. Gallier J., Bertault M. Freundlich P. and Kołodziej H.A., *Chem. Phys*., **229**, 275 (1998).
35. Noda I., *Appl. Spectr*., **51**, 994 (2000).
36. Skapski A.C. and Stevenson J.L., *J. Chem. Soc. Perkin Trans. II*, 1197 (1972).

37. Szostak M.M., Misiaszek T. and Roszak S., to be published.
38. Nobutoki H. and Koezuka H., *J. Phys. Chem. A*, **101**, 3762 (1997).
39. Szczęśniak M.M. and Scheiner S., *J. Phys. Chem*., **89**, 1835 (1985).
40. Trueblood K.N., Goldish E. and Donohue J., *Acta Cryst*., **14**, 1009 (1961).
41. Szostak M.M. and Rohleder J.W., *Acta Phys. Polon*., **37**, 521 (1970).
42. Lautié A., Froment F. and Novak A., *Spectr. Lett.*, **9**, 289 (1976).
43. Fillaux F., Fontaine J.P., Baron M.H., Kearley G.J. and Tomkinson J., *Chem. Phys*., **176**, 249 (1993).
44. Panunto T.W., Urbańczyk-Lipkowska Z., Johnson R. and Etter M.C., *J. Am. Chem. Soc*., **109**, 7786 (1987).
45. Knop E., Latanowicz L. and Reynhardt E.C., *Ber. Eunsenges. Phys. Chem*., **97**, 1457 (1993).
46. Tripathi G.N.R., Chipman D.M., Miderski C.A., Davis H.F., Fesseden R.W. and Schuler R.W., *J. Phys. Chem*., **90**, 3968 (1986).
47. Pan J. and Haarer D., *Chem. Phys. Lett*., **324**, 411 (2000).
48. Mitani T., *Mol. Cryst. Liq. Cryst*., **171**, 343 (1989).
49. Wójcik G. and Holband J., *Acta Cryst. E*, **57**, 346 (2001).
50. Katrusiak A., *Phys. Rev. Lett*., **77**, 4366 (1996).